# Stable Cationic Nanobelts Synthesized by Chemical Oxidation of Methylene-bridged [6]Cycloparaphenylene

Nobushige Kai,[†] Hideya Kono,[†] Timo Stünkel,[†] Daiki Imoto,[†] Riccardo Zanasi,*[,∇] Guglielmo Monaco,[∇] Francesco F. Summa,[∇] Lawrence T. Scott,[§] Akiko Yagi,*[,†,‡] and Kenichiro Itami*[,‡,°]

[†] Department of Chemistry, Graduate School of Science, Nagoya University, Nagoya 464-8602, Japan.

[‡] Institute of Transformative Bio-Molecules (WPI-ITbM), Nagoya University, Nagoya 464-8602, Japan.

[∇] Dipartimento di Chimica e Biologia "A. Zambelli", Università degli Studi di Salerno, Fisciano 84084, SA, Italy.

[§] Department of Chemistry, University of Nevada, Reno, Nevada 89557-0216, USA.

[°] Molecule Creation Laboratory, RIKEN Cluster for Pioneering Research, RIKEN, Wako, Saitama 351-0198, Japan.

KEYWORDS: Nanobelt, Methylene-bridged cycloparaphenylenes, Dication, Radical cation, Diatropic belt current

**ABSTRACT:** Cationic molecules have distinct properties that differ from those of electronically neutral molecules. They have been extensively studied and utilized as reaction intermediates, organic salts, and dyes. Among them, cationic arenes are of particular interest because they can act as charge carrier intermediates in p-type organic semiconductors. Although heteroatom-containing cationic arenes have been reported, those without heteroatoms, namely cationic aromatic hydrocarbons, are still rare and relatively unexplored due to their instability in air. Nanobelts are cyclic arenes that only consist of annulated structures. Recently, various types of nanobelts have been synthesized, and several unique properties of nanobelts have been unveiled. However, cationic nanobelts without heteroatoms have never been synthesized, and their properties are of significant interest from both fundamental and application perspectives. Herein, we report the first synthesis of cationic hydrocarbon nanobelts (radical cation and dication) obtained via the chemical oxidation of methylene-bridged [6]cycloparaphenylene ([6]MCPP). These cationic species turned out to be remarkably stable in air, which made it possible to measure and uncover their structural and electronic properties. Notably, the [6]MCPP dicationic salt has sharp absorption and fluorescence bands at much longer wavelengths than those of neutral [6]MCPP, close to the near-infrared region. From both experimental and theoretical investigation, the existence of a strong diatropic belt current in [6]MCPP dication has been indicated. In addition, a longer lifetime was observed for the hexamethyl[6]MCPP dicationic salt than for the [6]MCPP dicationic salt in solution. These findings regarding cationic hydrocarbon nanobelts contribute to a novel molecular design for stable cationic aromatic hydrocarbons.

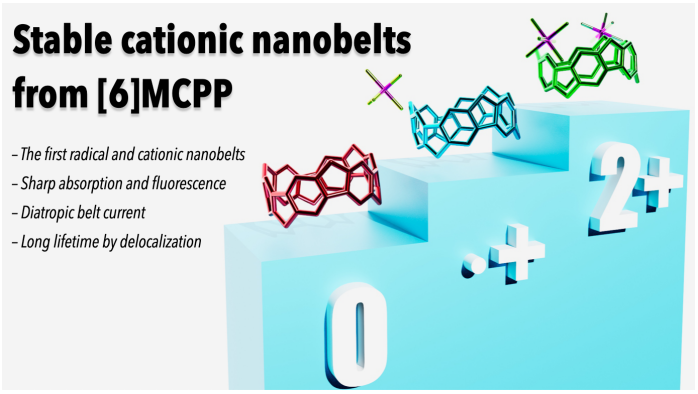


## INTRODUCTION

Cationic molecules have long been studied as reaction intermediates in a range of cation-triggered organic transformations and also have been utilized in numerous materials such as dyes, liquid crystals, conducting polymers, and photocatalysts.[1] Among them, cationic arenes, in which π-electrons have been removed from aromatic rings, have been recognized as important cationic molecules because they can act as intermediates of charge carriers in p-type organic semiconductors.[2] To utilize intrinsically moisture-sensitive cationic arenes as stable species, electron-donating heteroatoms such as nitrogen and oxygen atoms are often introduced into arene scaffolds. In contrast, cationic arenes without heteroatoms, namely cationic aromatic hydrocarbons, are rare.[3] While the introduction of multiple bulky substituents such as mesityl groups to gain air-stability has been a common strategy in the field, this generally cannot be applied to stabilize cations of π-conjugated arenes. Delocalization of positive charge is another powerful strategy for stabilizing cationic species of π-extended arenes. In the past decade, the groups of Jasti and Yamago have extensively studied the cationic species of cycloparaphenylenes (CPPs), revealing their unique size-dependent properties.[4] Considering the recent progress of the chemistry of π-extended arenes,[5] their cationic species are also worth investigating.

Nanobelts and aromatic belts are a class of synthetically challenging and recently emerging cyclic π-extended arenes (Figure 1a).[6,7] Since the first synthesis of (6,6)carbon nanobelts ((6,6)CNB) in 2017,[6] different types of nanobelts have been synthesized, and

their properties have been investigated. Despite the recent advances in nanobelts, cationic nanobelts are limited to certain dicationic species of nonalternant aromatic belts doped with nitrogen atoms.[8] There are no reports on the cationic species of hydrocarbon nanobelts, probably because of their assumed instability; thus, their synthesis is in strong demand.

Herein, we report the first synthesis of cationic hydrocarbon nanobelts. Methylene-bridged [6]cycloparaphenylene ([6]MCPP) was selected as our target nanobelt for obtaining a cationic nanobelt.[9] [6]MCPP is a nanobelt synthesized by our group in 2020, in which all the benzene rings of [6]CPP are bridged by methylene units. The synthesis of [6]MCPP requires only two steps from pillar[6]arene,[10] which has enabled the large-scale synthesis and commercialization of [6]MCPP.[11] Unique properties of [6]MCPP, such as a small energy gap (2.66 eV) and paratropic belt current, have led the progress of MCPP chemistry, as demonstrated by the syntheses of larger MCPPs ([8]MCPP and [10]MCPP),[12] a naphthalene-based MCPP,[13] and functionalized MCPPs.[14] Owing to the high highest occupied molecular orbital (HOMO) energy (–4.40 eV), electron-donating methylene units, and rigid cyclic π-conjugated system of [6]MCPP, we anticipated that cationic species of [6]MCPP can be easily and stably produced under air. The [6]MCPP radical cation $SbCl_6^-$ salt **1** and [6]MCPP dication $(SbF_6^-)_2$ salt **2** were synthesized and found to be very stable as solutions in $CH_2Cl_2$ and even as solids in air. Nuclear magnetic resonance (NMR) analysis, ultraviolet (UV)–visible (vis)–near-infrared region (NIR) absorption/fluorescence measurements, X-ray crystal structure analysis, and electron spin resonance (ESR) measurement of **1** and **2** revealed several unique properties of the cationic nanobelts.

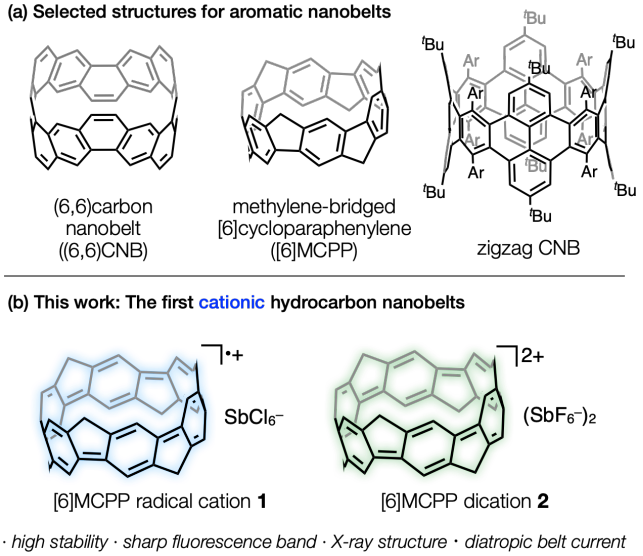


**Figure 1.** (a) The structures of neutral aromatic hydrocarbon nanobelts. Ar = *p*-$^t$BuC$_6$H$_4$. (b) The structures of [6]MCPP radical cation $SbCl_6^-$ salt **1** and [6]MCPP dication $(SbF_6^-)_2$ salt **2**.

## RESULTS AND DISCUSSION

### Syntheses of [6]MCPP cations

Chemical oxidation of [6]MCPP with 3 equivalents of $NOSbF_6$ in $CH_2Cl_2$ solution, at 23 °C under an argon atmosphere, changed the red color of the reaction solution, derived from [6]MCPP, to a yellow green color. From $^1$H NMR, $^{13}$C NMR, and electron spray ionization (ESI) mass spectrometric analyses, as well as UV–vis–NIR absorption measurements, the full conversion of [6]MCPP was observed and **2** was obtained in 92% yield (Scheme 1). When using 1 equivalent of $NOSbF_6$, the formation of **1** was indicated by the ESR and absorption spectra of the reaction mixture, while **2** was also present (see Supporting Information (SI) for details). By treating [6]MCPP with $Et_3OSbCl_6$, a slightly weaker oxidant than $NOSbF_6$ ($E_{ox}$; 0.87 V and 0.91 V (vs $Fc/Fc^+$), respectively), **1** was selectively obtained in $CH_2Cl_2$ at –78 °C. The reaction solution was warmed to 23 °C and exposed to air, followed by ESR analysis and absorption measurements to confirm the successful formation of **1**. The half-life of **1** and **2** are determined as about 143 hours and 26 hours, respectively, from the decay of the maximum absorption peak intensities in $CH_2Cl_2$ solution under air (see SI for details). The determined values of half-life should be longer than CPP cations, which are characterized as air-sensitive in reported papers.[4]

**Scheme 1.** Synthesis of **1** and **2**[a].

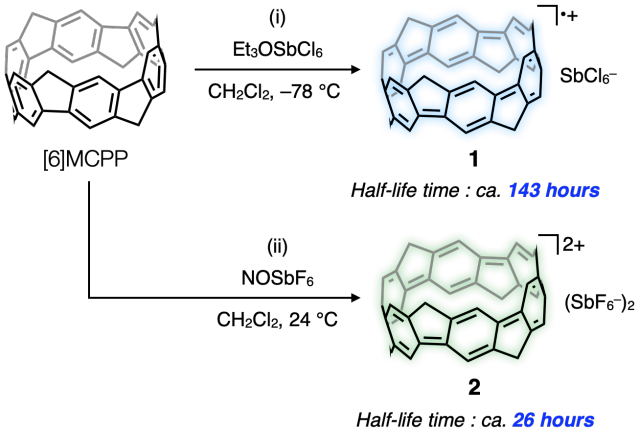


[a]Reaction conditions: (i) [6]MCPP (4.5 μmol, 2.4 mg, 1.0 equiv.), $Et_3OSbCl_6$ (3.6 μmol, 1.6 mg, 0.8 equiv.), $CH_2Cl_2$ (2.0 mL). (ii) [6]MCPP (7.6 μmol, 4.0 mg, 1.0 equiv.), $NOSbF_6$ (23 μmol, 6.0 mg, 2.2 equiv.), $CH_2Cl_2$ (3.0 mL). Half-life time was determined in $CH_2Cl_2$ solution at 23 °C under air.

### X-ray crystal structure of [6]MCPP dication 2

A single crystal of **2** was successfully obtained by slow evaporation of a $CH_2Cl_2$ solution at –30 °C under an argon atmosphere for 6 days. X-ray single-crystal structural analysis revealed the crystal structure of **2** (Figure 2a) and its packing structure, where the $[6]MCPP^{2+}$ scaffold is aligned in columns with two sandwiched $SbF_6^-$ anions and $CH_2Cl_2$ molecules (Figure 2b).[14] The diameter of the $[6]MCPP^{2+}$ scaffold is estimated as 7.675 Å, which is 0.083 Å shorter than that of neutral [6]MCPP (Table 1). Considering the carbon–carbon bonds, the difference between **2** and [6]MCPP strongly indicates that the $[6]MCPP^{2+}$ scaffold has a quinoidal character. The harmonic oscillator model of aromaticity (HOMA) values for the 6-membered rings are estimated using the crystal structures of [6]MCPP and **2**, and density functional theory (DFT) calculations at the B3LYP/6-31G(d) level of theory (see SI for details). The average HOMA value is 0.702 for $[6]MCPP^{2+}$ scaffold in contrast to 0.955 for [6]MCPP, supporting the increased quinoidal character of **2**. This difference was also observed in the case of cationic CPPs, which explains the effective delocalization of the positive charge across the entire $[6]MCPP^{2+}$ scaffold.

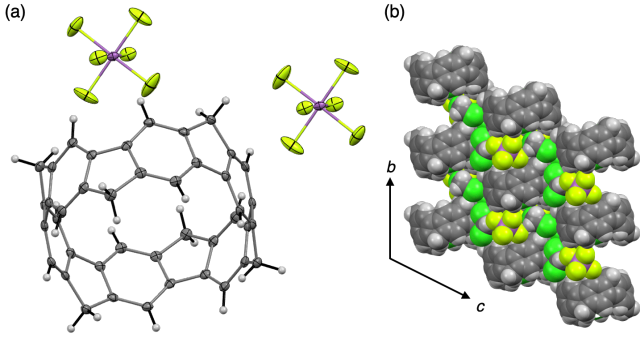


**Figure 2.** X-ray crystal structure of **2**. (a) Oak Ridge Thermal Ellipsoid Plot (ORTEP) drawing of **2** with 50% thermal probability. (b) Packing structure viewed along the *a*-axis.

**Table 1.** Structure index of **2** and comparison with [6]MCPP.

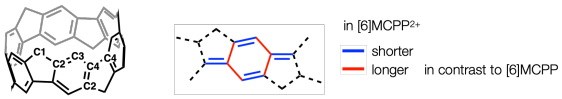


| | [6]MCPP | [6]MCPP$^{2+}$ | Δ([6]MCPP$^{2+}$–[6]MCPP) |
|---|---|---|---|
| Diameter [Å] | 7.758 | 7.675 | -0.083 |
| C1–C2 [Å] | 1.518 | 1.514 | -0.004 |
| C2–C3 [Å] | 1.384 | 1.368 | -0.016 |
| C2–C4 [Å] | 1.408 | 1.436 | 0.028 |
| C3–C4 [Å] | 1.395 | 1.415 | 0.020 |
| C4–C4 [Å] | 1.478 | 1.428 | -0.050 |

## Photophysical properties of [6]MCPP cations

The UV–vis–NIR absorption and fluorescence spectra of **1** and **2,** in $CH_2Cl_2$ solutions, are recorded and compared with those of [6]MCPP (Figure 3a). For **1**, four absorption peaks are observed at 415, 870, 1037, and 1054 nm. The absorption band in the NIR region clearly indicates the radical cationic character of **1**, which undergoes transitions with a singly occupied molecular orbital (SOMO). Using DFT calculations, the frontier molecular orbitals of **1** and **2** were depicted to reveal that the SOMO of **1** is distributed exactly the same way as the HOMO of [6]MCPP, and the other frontier molecular orbitals of **1** are shifted by one (see Figure 3b and SI). Similarly, the LUMO of **2** has the same orbital distribution as that of the HOMO of [6]MCPP, whereas the other orbitals are shifted by one. The absorption bands of **1**, with peaks at approximately 415 nm and 1040 nm can be attributed to HOMO/HOMO–1 to LUMO and HOMO/HOMO–1 to SOMO transitions, respectively, as estimated by time-dependent DFT (TDDFT) calculation at the UB3LYP/6-31G(d) level of theory. Fluorescence of the $CH_2Cl_2$ solution of **1** was not observed.

The absorption bands of the $CH_2Cl_2$ solution of **2** are observed with peaks at 453 and 745 nm. The positions of the peaks correspond well with the HOMO/HOMO–1→LUMO+1 (415 nm) and HOMO/HOMO–1→LUMO (701 nm) transitions calculated using TDDFT. Notably, the absorption band with a peak around 745 nm is very sharp with a full width at half maximum (FWHM) of 14.5 nm. The fluorescence spectrum of **2** was observed, whereas neutral [6]MCPP exhibited negligible fluorescence due to forbidden transitions. The FWHM of the fluorescence band of **2** is also small (20 nm), comparable to that of quantum dots or dyes with heteroatoms.[15] The fluorescence quantum yield ($\Phi_F$) of **2** is determined to be 0.23. Considering that the Stokes shift is only 5 nm and self-absorption is not negligible, the value of $\Phi_F$ is siginificant. Compared to [6]CPP$^{2+}$·$(SbF_6^-)_2$ $CH_2Cl_2$ solution, **2** has over 10 times larger $\Phi_F$ (0.23 vs. 0.018).[4f] The oscillator strengths ($f$) for fluorescence of **2** and [6]CPP$^{2+}$·$(SbF_6^-)_2$ were estimated to be 0.22 and 0.20, respectively, from TDDFT calculation based on the optimized structures of $S_1$ states for [6]MCPP$^{2+}$ and [6]CPP$^{2+}$ (see SI for details). Because $\Phi_F$ is defined as $k_f/(k_f + k_{nd} + k_{ISC})$, where $k_f$ is fluorescence rate, $k_{nd}$ is nonradiative deactivation rate, $k_{ISC}$ is intersystem crossing rate, and $k_{ISC}$ is negligible for [6]MCPP$^{2+}$ and [6]CPP$^{2+}$, the difference in $\Phi_F$ may be due to $k_{nd}$. Nonradiative deactivation, particularly thermal deactivation, is expected be small in the [6]MCPP$^{2+}$ scaffold compared to [6]CPP$^{2+}$ by virtue of the rigid structure resulting from the methylene bridges. These results clearly show that methylene-bridging modulates the spectroscopic properties of the parent [6]CPP dication structure, enabling fluorescense, which is a remarkable structural effect of methylene-bridging firstly revealed by this work.

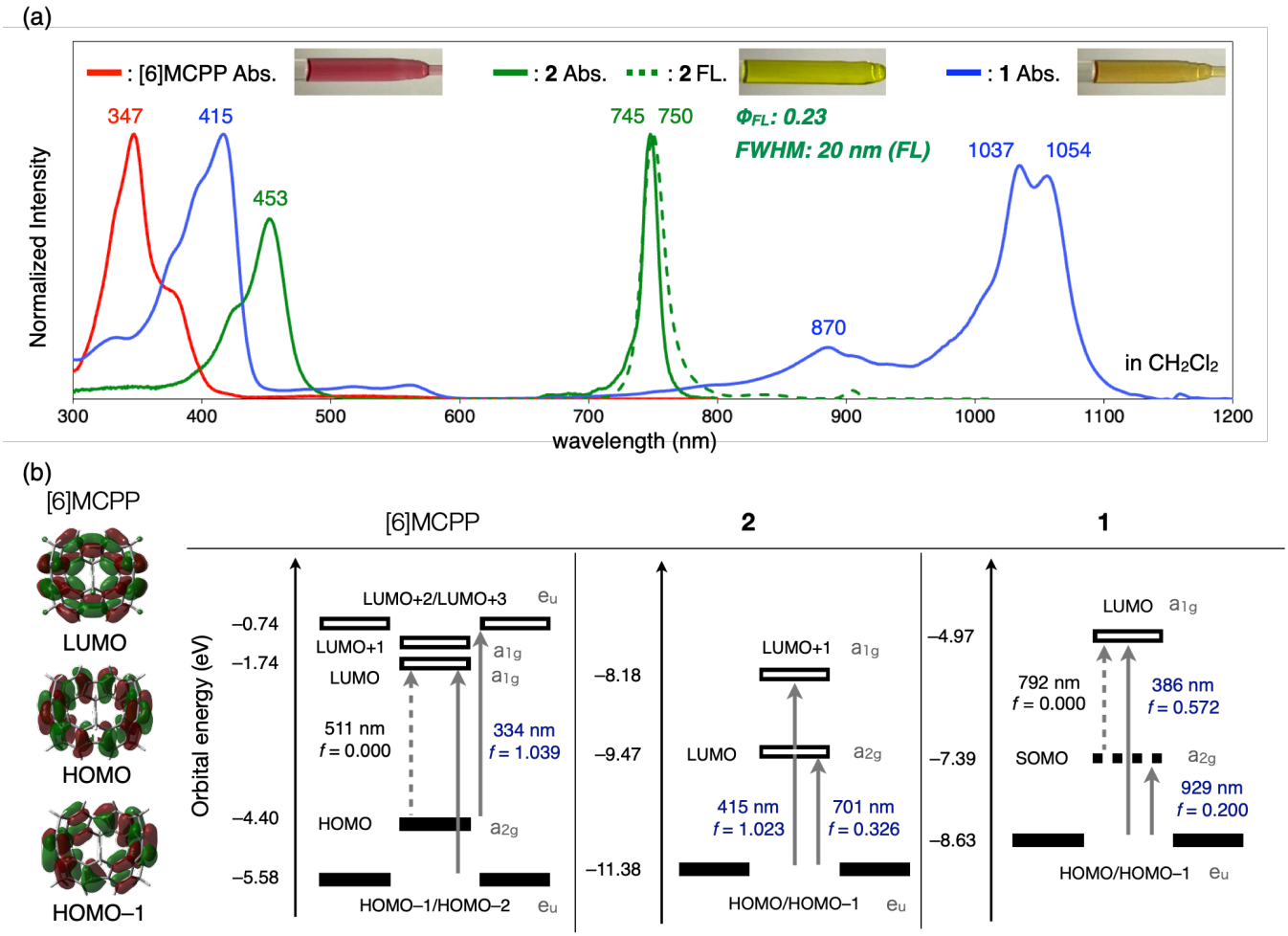


**Figure 3.** (a) UV–vis–NIR absorption (solid line) and fluorescence (dashed line) spectra of $CH_2Cl_2$ solutions of [6]MCPP, **1**, and **2**. Fluorescence spectrum of **2** was recorded upon excitation at 450 nm. (b) Frontier molecular orbitals of [6]MCPP and transitions estimated by TDDFT calculation.

## NMR analysis of [6]MCPP dication

In our previous work, the paratropic belt current of MCPP, which changes depending on the ring size, was first unveiled.[11] The chemical shifts of the methylene hydrogen atoms in $^1$H NMR spectra indicate the existence of a paratropic belt current that decreases with increasing ring size of [*n*]MCPP (*n* = 6, 8, and 10), which is also supported by a theoretical study of the magnetically induced current density. To investigate the belt-current effect in the [6]MCPP$^{2+}$ scaffold, the $^1$H NMR spectrum of **2** in $CD_2Cl_2$ was recorded (Figure 4). As observed for neutral [6]MCPP, **2** also exhibited three types of signals: a singlet signal at 4.18 ppm, two doublet signals at 3.61 ppm and –0.34 ppm. This suggests a $D_{3d}$ symmetry for **2** in $CH_2Cl_2$ solution, indicating a delocalized positive charge on the entire [6]MCPP$^{2+}$ scaffold. The observed chemical shifts of the signals were further supported by simulations using gauge-including atomic orbitals (GIAO) calculations at the B3LYP/6-311+G(2d,p) level (see SI for details). The singlet signal of 4.18 ppm is assigned to the hydrogen atoms on benzene rings (highlighted as green color in Figure 4). The doublet signal of 3.61 ppm is assigned to the methylene hydrogen atoms facing outside of nanobelt ($H_{out}$, highlighted as red color) and the doublet signal of –0.34 ppm is from those facing inside of nanobelt ($H_{in}$, highlighted as blue color).

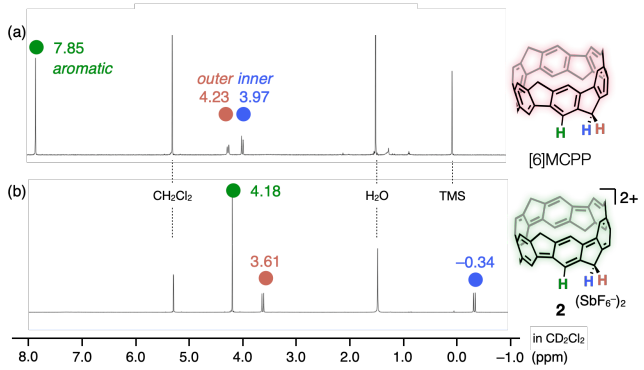


**Figure 4.** $^1$H NMR spectra of (a) [6]MCPP and (b) **2** at 600 MHz. TMS: tetramethylsilane.

## NMR theoretical study

The extraordinary upfield shift of the $^1$H NMR signals of **2** can only be attributed to a drastic change in the current regime induced by the magnetic field of the spectrometer. As we will show in the following, the paratropic belt current that characterizes the magnetic response of [6]MCPP disappears in the dication, giving way to an intense diatropic belt current that causes a large anisotropic effect on

the $^1$H NMR signals. The deshielding effect is particularly pronounced for $H_{in}$, whose δ moves up-field by 4.41 ppm. The aromatic hydrogen atoms undergo a similar shift equal to 3.67 ppm, while $H_{out}$ moves only 0.62 ppm for their external disposition.

Magnetically-induced electron current density and aryl–aryl bond current strength of **2** have been calculated assuming the combination B97-2/6-311+G(2d,p) of density functional and basis set, using the SYSMOIC program package as in previous studies.[17a] The wave functions for the calculation have been obtained using the G16 program package,[17b] including, in this case of a charged molecule, the solvent ($CH_2Cl_2$) effect by means of the CPCM method.[17c]

We find that the dominant contribution to the delocalized electron current density is given by the HOMO. This contribution is shown in Figure 5. To facilitate the comparison with [6]MCPP, two values of the filter that cuts the low magnitude current have been adopted. The Figure 5 top is identical to that used for depiction of the belt current in [6]MCPP, i.e., 0.015 a.u.. The Figure 5 bottom has been set to 0.04 a.u. to clearly show the current and how its flow bifurcates and gathers around the six-membered rings of the nanobelts.

First, we observe the opposite direction of circulation of the current compared to that of the neutral species, i.e., diatropic instead of paratropic; second, the magnitude of the current is much larger. To obtain a quantitative estimate, bond current strengths[17d] have been calculated, integrating the current crossing a 5×5 a.u. square perpendicular to one aryl–aryl bond in its middle (shown in red in Figure 5) for the three instances: only HOMO, all-but-HOMO, all-MOs. Values are reported in Table 2 as a percentage of the benzene ring current strength ($I_{BEN}$) calculated using the same method, i.e., $I/|I_{BEN}| \times 100$, with IBEN=12 nA/T. Customarily, the sign of the $I_{BEN}$ is taken as negative, so that paratropic/diatropic current strengths are identified by a positive/negative sign.[17e]

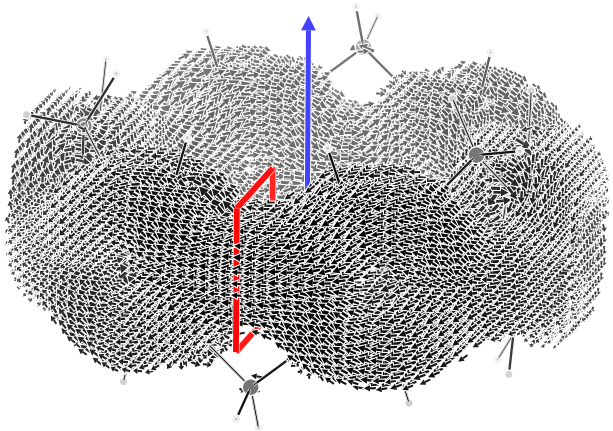

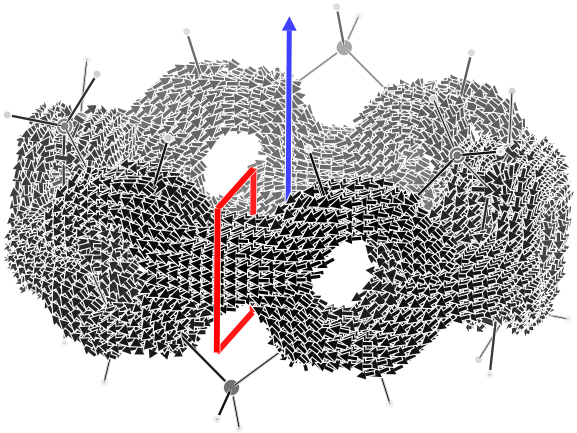

**Figure 5**. HOMO contribution to the electron current density induced in **2** by a magnetic field parallel to the main symmetry axis (blue arrow). Top/bottom current lower than 0.015/0.04 a.u. are not shown. Maximum current is 0.34 a.u.. Red square delimits the integration region for the calculation of aryl–aryl bond current strength.

**Table 2**. Belt signed current strength (aryl–aryl) in percentage of the benzene bond current strength calculated using same method.

| Molecule | HOMO | All-but-HOMO | All-MOs |
|---|---|---|---|
| **2** | –241 | –1 | –242 |
| [6]MCPP | +138 | –63 | +75 |

As it can be seen, the delocalized diatropic belt current of **2** is almost entirely due to the HOMO. Two contributions were instead found for [6]MCPP, one dominant paratropic and another less intense diatropic. All that can be very easily understood by considering the symmetries of the frontier molecular orbitals shown in Figure 3.

According to the few electrons model by Steiner and Fowler,[17f,g] an occupied-to-unoccupied virtual transition gives a paratropic contribution if the product of symmetries contains a match to a rotation, and a diatropic contribution if it contains a match to a translation. For [6]MCPP the HOMO→LUMO transition ($a_{2g} \otimes a_{1g} = a_{2g}$) gives the already well-known paratropic belt current whose strength is 138% of $|I_{BEN}|$, while the HOMO-1→LUMO transition ($e_u \otimes a_{1g} = e_u$) makes a contribution that accounts almost entirely for the diatropic contribution of –63% of $|I_{BEN}|$. The smaller HOMO-LUMO gap is consistent with the bigger paratropic contribution. Now, as already observed above, the HOMO of [6]MCPP becomes the LUMO of **2**. Thus, two transitions originate from the HOMO of the dication ($e_u \otimes a_{2g} = e_u$ and $e_u \otimes a_{1g} = e_u$) which give the large diatropic belt current shown in Figure 5, whose strength is estimated to be -242% of $|I_{BEN}|$.

## Further study toward a stable MCPP dication

The interesting properties of **1** and **2** described above are unveiled owing to their high stability as both solution and solid under air. In order to discuss the extraordinarily high stability of **2**, the chemical oxidation of hexamethyl[6]MCPP, which is a known molecule reported in 2021,[14a] has been tried in a same manner as the synthesis of **2**. The dicationic species of hexamethyl[6]MCPP **3** has been obtained successfully to investigate its half-life time in $CH_2Cl_2$

solution under air. As a result, it was found that **3** has a much longer half-life time than **2**, which is estimated to be about 2640 hours (110 days). Although discussion for high stability was difficult because neither $^{13}C$ NMR analysis nor X-ray diffraction analysis was successful, kinetic protection, electron-donating effect and hyperconjugation effect of methyl groups likely improve the stability of [6]MCPP dication.

**Scheme 2.** Chemical oxidation of hexamethyl[6]MCPP.

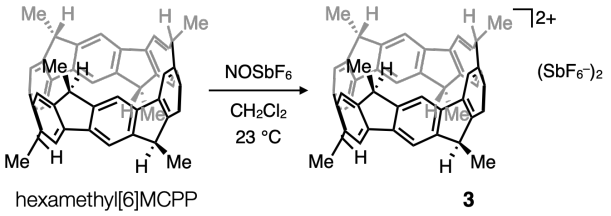


[a]Reaction conditions: hexamethyl[6]MCPP (7.6 μmol, 4.6 mg, 1.0 equiv.), $NOSbF_6$ (23 μmol, 6.0 mg, 3.0 equiv.), $CH_2Cl_2$ (3.0 mL). Half-life time was elucidated in $CH_2Cl_2$ solution at 23 °C under air.

## CONCLUSION

In conclusion, we have synthesized [6]MCPP radical cationic salt **1** and [6]MCPP dicationic salt **2** from [6]MCPP. The appropriate choice of chemical oxidants has led the successful synthesis of the [6]MCPP cationic species. The half-life times of the cationic species are longer than those of CPP cationic species, possibly owing to the methylene-bridged structures which fix the quinoidal CPP structure to a belt form. As important properties of [6]MCPP cations, we found that the crystal structure of **2** has an obvious quinoidal character and a smaller diameter in contrast to neutral [6]MCPP. The UV–vis–NIR absorption and fluorescence spectra of **2** have small FWHM in long wavelength close to NIR, which indicates the possibility of **2** to be used as a unique photo material. The drastic change in the fluorescence quantum yields of **2** ($\Phi_F$ = 0.23) and neutral [6]MCPP ($\Phi_F \sim 0$) means that turning the fluorescence on and off is possible by using oxidation of [6]MCPP. Notably, experimental and theoretical $^1H$ NMR studies of **2** uncovered its interesting magnetic property: a diatropic belt current. The belt current of **2** is much stronger than that of [6]MCPP, which is reasonable from allowed transition in frontier molecular orbitals of **2**. In order to create highly stable MCPP dications, hexamethyl[6]MCPP has been oxidized similarly. The thus-obtained dication **3** was extraordinarily stable to strongly indicate the hyperconjugation effect, electron-donating effect and kinetic protection by the methyl groups in **3**. The compounds synthesized in this study are the first radical and cationic nanobelts so far. Their striking properties would give new insights into the chemistry of π-conjugated molecules and materials science.

## ASSOCIATED CONTENT

### Supporting Information

The Supporting Information is available free of charge on the ACS Publications website at DOI: XXXX.

Experimental procedures, $^1H$ and $^{13}C$ NMR spectra, characterization data for all new compounds, optical properties, computational data, and crystallographic data of **2** (PDF)
X-ray crystallographic data for **2** (CIF).

## AUTHOR INFORMATION

### Corresponding Authors

Riccardo Zanasi – Dipartimento di Chimica e Biologia "A. Zambelli", Università Degli Studi di Salerno, Fisciano, Salerno 84084, Italy; Email: rzanasi@unisa.it

Akiko Yagi – Department of Chemistry, Graduate School of Science and Institute of Transformative Bio-Molecules (WPI-ITbM), Nagoya University, Nagoya 464-8602, Japan; Email: yagi.akiko@itbm.nagoya-u.ac.jp

Kenichiro Itami – Molecule Creation Laboratory, RIKEN Cluster for Pioneering Research, Wako, Saitama 351-0198, Japan.; Email: kenichiro.itami@riken.ac.jp

### Authors

Nobushige Kai – Department of Chemistry, Graduate School of Science, Nagoya University, Nagoya 464-8602, Japan.

Hideya Kono – Department of Chemistry, Graduate School of Science, Nagoya University, Nagoya 464-8602, Japan.

Timo Stünkel – Department of Chemistry, Graduate School of Science, Nagoya University, Nagoya 464-8602, Japan.

Daiki Imoto – Department of Chemistry, Graduate School of Science, Nagoya University, Nagoya 464-8602, Japan.

Guglielmo Monaco – Dipartimento di Chimica e Biologia "A. Zambelli", Università Degli Studi di Salerno, Fisciano, Salerno 84084, Italy.

Francesco F. Summa – Dipartimento di Chimica e Biologia "A. Zambelli", Università Degli Studi di Salerno, Fisciano, Salerno 84084, Italy.

Lawrence T. Scott – Department of Chemistry, University of Nevada, Reno, Nevada 89557-0216, USA.

### Author Contributions

The manuscript was written through contributions of all authors.

### Funding Sources

This work is supported by JSPS Promotion of Joint International Research (grant number 22K21346 to A.Y.) and Sumitomo Foundation (to A.Y.).

## ACKNOWLEDGMENT

We thank Dr. Kin-ichi Oyama and Ms. Rio Yamada (Nagoya University) for their support in ESI-MS measurement and analysis. We also thank Ms. Yui Ito, Associate Prof. Masahito Murai and Prof. Shigehiro Yamaguchi (Nagoya University) for their support in NIR absorption and FL measurements. The authors also thank Dr. Hiroki Shudo (Nagoya University) for fruitful discussion. H.K. and D.I. thank the Nagoya University Graduate Program of Transformative Chem-Bio Research (WISE Program) supported by MEXT. T.S. thanks and the Deutsche

Forschungsgemeischaft (DFG, German Research Foundation - GRK2678-437785492). Computations were performed using the resources of the Research Center for Computational Science, Okazaki, Japan (23-IMS-C087 and 24-IMS-C123).

## REFERENCES


1. (a) Peters, S, K. Nature of Dynamic Processes Associated with the $S_N1$ Reaction Mechanism. *Chem. Rev.* **2007**, *107*, 859–873. (b) Heinze, J.; Frontana-Uribe, B. A.; Ludwigs, S. Electrochemistry of Conducting Polymers–Persistent Models and New Concepts. *Chem. Rev.* **2010**, *110*, 4724–4771. (c) Bosson, J.; Gouin, J.; Lacour, J. Cationic triangulenes and helicenes: synthesis, chemical stablity, optical properties and extended applications of these unusual dyes. *Chem. Soc. Rev.* **2014**, *43*, 2824–2840. (d) Goosens, K.; Lava, K.; Bielawski, C. W.; Binnemans, K. Ionic Liquid Crystals: Versatile Materials. *Chem. Rev.* **2016**, 116, 4643–4807 (e) Romero, N. A.; Nicewicz, D. A. Organic Photoredox Catalysis. *Chem. Rev.* **2016**, *116*, 10075–10166.
2. (a) Nishinaga, T. Organic Redox Systems, John Wiley & Sons, Inc, Hoboken, NJ, 2015. (b) Antoni, P. W.; Hansmann, M. M. Pyrylenes: A New Class of Tunable, Redox-Switchable, Photoexcitable Pyrylium–Carbene Hybrids with Three Stable Redox-States. *J. Am. Chem. Soc.* **2018**, *140*, 14823–14835. (c) Harimoto, T.; Ishigaki, Y. Redox-Active Hydrocarbons: Isolation and Structural Determination of Cationic States toward Advanced Response Systems. *ChemPlusChem* **2022**, *87*, e202200013.
3. (a) Matsuura, A.; Nishinaga, T.; Komatsu, K. Structural Studies on the Radical Cations of Benzene, Naphthalene, Biphenylene, and Anthracene Fully Annelated with Bicyclo[2.2.2]octene Frameworks. *J. Am. Chem. Soc.* **2000**, *122*, 10007–10016. (b) Komatsu, K.; Aonuma, S.; Jinbu, Y.; Tsuji, R.; Hirokawa, C.; Takeuchi, K. Generation and Oligomerization of Bicyclo[2.2.2]octyne and Properties of Tris(bicyclo[2.2.2]octeno)benzene Obtained from the Linear Trimer. *J. Org. Chem.* **1991**, *56*, 195–203. (c) Banerjee, M.; Vyas, V, S.; Lindeman, S, V.; Rathore, R. Isolation and X-ray structural characterization of tetraisopropylpyrene cation radical. *Chem. Commun.* **2008**, 1889–1891. (d) Banerjee, M.; Shukla, R.; Rathore, R. Synthesis, Optical, and Electronic Properties of Soluble Poly-*p*-phenylene Oligomers as Models for Molecular Wires. *J. Am. Chem. Soc.* **2009**, *131*, 1780–1786. (e) Nishiuchi, T.; Aibara, S.; Kubo, T. Synthesis and Properties of a Highly Congested Tri(9-anthryl)methyl Radical. *Angew. Chem., Int. Ed.* **2018**, *57*, 16516–16519. (f) Zhu, C.; Shoyama, K.; Würthner, F. Conformation and Aromaticity Switching in a Curved Non-Alternant $sp^2$ Carbon Scaffold. *Angew. Chem., Int. Ed.* **2020**, *59*, 21505–21509. (g) Ishigaki, Y.; Harimoto, T.; Sugawara, K.; Suzuki, T. Hysteretic Three-State Redox Interconversion among Zigzag Bisquinodimethanes with Non-fused Benzene Rings and Twisted Tetra-/Dications with [5]/[3]Acenes Exhibiting Near-Infrared Absorptions. *J. Am. Chem. Soc.* **2021**, *143*, 3306–3311. (h) Miyoshi, H.; Sugiura, R.; Kishi, R.; Spisak, S. N.; Wei, Z.; Muranaka, A.; Uchiyama, M.; Kobayashi, N.; Chatterjee, S.; Ie, Y.; Hisaki, I.; Petrukhina, M. A.; Nishinaga, T.; Nakano, M.; Tobe, Y. Dianion and Dication of Tetracyclopentatetraphenylene as Decoupled Annulane-within-an-Annulene Models. *Angew. Chem., Int. Ed.* **2022**, *61*, e202115316. (i) Li, Z.; Hou, X.; Han, Y.; Fan, W.; Ni, Y.; Zhou, Q.; Zhu, J.; Wu, S.; Huang, K. Wu, J. [8]Cyclo-*para*-phenylmethine as a Super-Cyclooctatetraene: Dynamic Behavior, Global Aromaticity, and Open-Shell Diradical Character in the Neutral and Dicationic States. *Angew. Chem., Int. Ed.* **2022**, *61*, e202210697. (j) Yoshihara, T.; Shudo, H.; Yagi, A.; Itami, K. Adamantane Annulation to Arenes: A Strategy for Property Modulation of Aromatic π-Systems. *J. Am. Chem. Soc.* **2023**, *145*, 11754–11763.
4. (a) Golder, M, R.; Wong, B, M.; Jasti, R. Photophysical and theoretical investigations of the [8]cycloparaphenylene radical cation and its charge-resonance dimer. *Chem. Sci.* **2013**, *4*, 4285–4291. (b) Kayahara, E.; Kouyama, T.; Kato, T.; Takaya, H.; Yasuda, N.; Yamago, S. Isolation and Characterization of the Cycloparaphenylene Radical Cation and Dication. *Angew. Chem., Int. Ed.* **2013**, *52*, 13722–13726. (c) Toriumi, N.; Muranaka, A.; Kayahara, E.; Yamago, S.; Uchiyama, M. In-Plane Aromaticity in Cycloparaphenylene Dications: A Magnetic Circular Dichroism and Theoretical Study. *J. Am. Chem. Soc.* **2015**, *137*, 82–85. (d) Kayahara, E.; Kouyama.; T, Kato, T.; Yamgo, S. Synthesis and Characterization of [*n*]CPP (*n* = 5, 6, 8, 10, and 12) Radical Cation and Dications: Size-Dependent Absorption, Spin, and Charge Delocalization. *J. Am. Chem. Soc.* **2016**, *138*, 338–344. (e) Alvarez, M. P.; Ruiz Delgado, M. C.; Taravillo, M.; Baonza, V. G.; Lopez Navarrete, J. T.; Evans, P.; Jasti, R.; Yamago, S.; Kertesz, M.; Casado, J. The Raman fingerprint of cyclic conjugation: the case of the stabilization of cations and dications in cycloparaphenylenes. *Chem. Sci.* **2016**, *7*, 3494–3499. (f) Matsumoto, Y.; Toriumi, N.; Muranaka, A.; Kayahara, E.; Yamago, S.; Uchiyama, M. Near-Infrared Fluorescence from In-Plane-Aromatic Cycloparaphenylene Dications. *J. Phys. Chem. A* **2018**, *122*, 5162–5167.
5. (a) Segawa, Y.; Ito, H.; Itami, K. Structurally uniform and atomically precise carbon nanostructures. *Nat. Rev. Mater.* **2016**, *1*, 15002. (b) Segawa, Y.; Levine, D. R.; Itami, K. Topologically Unique Molecular Nanocarbons. *Acc. Chem. Res.* **2019**, *52*, 2760–2767. (c) Panwar, N.; Soehartono, A. M.; Chan, K. K.; Zeng, S.; Xu, G.; Qu, J.; Coquet, P.; Yong, K-T.; Chen, X. Nanocarbons for Biology and Medicine: Sensing, Imaging, and Drug Delivery. *Chem. Rev.* **2019**, *119*, 9559–9656. (d) Tielens, A. G. G. M. Interstellar Polycyclic Aromatic Hydrocarbon Molecules. *Annu. Rev. Astron. Astrophys.* **2008**, 46, 289–337. (e) Harvey, R. G. Polycyclic Aromatic Hydrocarbons, Wiley-VCH, New York, 1997. (f) Narita, A.; Wang, X. Y.; Feng, X.; Müllen, K. New advances in nanographene chemistry. *Chem. Soc. Rev.* **2015**, *44*, 6616–6643. (g) Yoon, K.-Y.; Dong, G. Liquid-phase bottom-up synthesis of graphene nanoribbons. *Mater. Chem. Front.* **2020**, *4*, 29–45.
6. Povie, G.; Segawa, Y.; Nishihara, T.; Miyauchi, Y.; Itami, K. Synthesis of a carbon nanobelt. *Science* **2017**, *356*, 172–175.
7. (a) Lewis, S. E. Cycloparaphenylenes and Related Nanohoops. *Chem. Soc. Rev.* **2015**, *44*, 2221–2304. (b) Segawa, Y; Yagi, A.; Matsui, K.; Itami, K. Design and Synthesis of Carbon Nanotube Segments. *Angew. Chem., Int. Ed.* **2016**, *55*, 5136–5158. (c) Guo, Q. H.; Qiu, Y.; Wang, M. X.; Stoddart, J. F. Aromatic hydrocarbon belts. *Nat. Chem.* **2021**, *13*, 402–419. (d) Imoto, D.; Yagi, A.; Itami, K. Carbon Nanobelts: Brief History and Perspective. *Precis. Chem.* **2023**, *1*, 516–523.
8. Sato, H.; Suizu, R.; Kato, T.; Yagi, A.; Segawa, Y.; Awaga, K.; Itami, K. N-doped nonalternant aromatic belt via a six-fold annulative double N-arylation. *Chem. Sci.* **2022**, *13*, 9947–9951.
9. Li, Y.; Segawa, Y.; Yagi, A.; Itami, K. A Non-alternant Aromatic Belt: Methylene-bridged [6]Cycloparaphenylene Synthesized from Pillar[6]arene. *J. Am. Chem. Soc.* **2020**, *142*, 12850–12856.
10. (a) Ogoshi, T.; Kanai, S.; Fujinami, S.; Yamagishi, T.; Nakamoto, Y. *para*-Bridged Symmetrical Pillar[5]arenes: Their Lewis Acid Catalyzed Synthesis and Host–Guest Property**.** *J. Am. Chem. Soc.* **2008**, *130*, 5022–5023. (b) Ogoshi, T.; Yamagishi, T.; Nakamoto, Y. Pillar-Shaped Macrocyclic Hosts Pillar[*n*]arenes: New Key Players for Supramolecular Chemistry. *Chem. Rev.* **2016**, *116*, 7937–8002.
11. https://www.tcichemicals.com/assets/brochure-pdfs/Brochure_FF122_E.pdf
12. Kono, H.; Li, Y.; Zanasi, R.; Monaco, G.; Summa, F. F.; Scott, L. T.; Yagi, A.; Itami, K. Methylene-Bridged [6]-, [8]-, and [10]Cycloparaphenylenes: Size-Dependent Properties and Paratropic Belt Currents. *J. Am. Chem. Soc.* **2023**. *145*, 8939–8946.
13. Kai, N.; Kono, H.; Yagi, A.; Itami, K. Synthesis and Properties of Methylene-Bridged [6]Cyclo-2,6-Naphthylene. *Synlett* **2023**, *34*, 1433–1436.
14. (a) Du, X.-S.; Zhang, D.-W.; Guo, Y.; Li, J.; Han, Y.; Chen, C.-F. Towards the Highly Efficient Synthesis and Selective Methylation of C($sp^3$)-Bridged [6]Cycloparaphenylenes from Fluoren[3]arenes. *Angew. Chem., Int. Ed.* **2021**, *60*, 13021–13028. (b) Zhang, F.; Du, X.-S.; Zhang, D.-W.; Wang, Y.-F.; Lu, H.-Y.; Chen, C.-F. A Green Fluorescent Nitrogen-Doped Aromatic Belt Containing a [6]Cycloparaphenylene Skeleton. *Angew. Chem., Int. Ed.* **2021**, *60*, 15291-15295.
15. CCDC number of **2**: 2359239

16. (a) Pietryga, J. M.; Park, Y. S.; Lim, J.; Fidler, A. F.; Bae, W. K.; Broveli, S.; Klimov, V. I. Spectroscopic and Device Aspects of Nanocrystal Quantum Dots. *Chem. Rev.* **2016**, *116*, 10513–10622. (b) Zhao, W.; Carreira, E. M. Conformationally Restricted Aza-BODIPY: Highly Fluorescent, Stable Near-Infrared Absorbing Dyes. *Angew. Chem., Int. Ed.* **2005**, *44*, 1677–1679.

17. (a) Monaco, G.; Summa, F. F.; Zanasi, R. Program Package for the Calculations of Origin-Independent Electron Current Density and Derived Magnetic Properties in Molecular Systems. *J. Chem. Inf. Model.* **2021**, *61*, 270–283. (b) Frisch, M. J.; Trucks, G. W.; Schlegel, H. B.; Scuseria, G. E.; Robb, M. A.; Cheeseman, J. R.; Scalmani, G.; Barone, V.; Petersson, G. A.; Nakatsuji, H.; Li, X.; Caricato, M.; Marenich, A. V.; Bloino, J.; Janesko, B. G.; Gomperts, R.; Mennucci, B.; Hratchian, H. P.; Ortiz, J. V.; Izmaylov, A. F.; Sonnenberg, J. L.; Williams-Young, D.; Ding, F.; Lipparini, F.; Egidi, F.; Goings, J.; Peng, B.; Petrone, A.; Henderson, T.; Ranasinghe, D.; Zakrzewski, V. G.; Gao, J.; Rega, N.; Zheng, G.; Liang, W.; Hada, M.; Ehara, M.; Toyota, K.; Fukuda, R.; Hasegawa, J.; Ishida, M.; Nakajima, T.; Honda, Y.; Kitao, O.; Nakai, H.; Vreven, T.; Throssell, K.; Montgomery, Jr., J. A.; Peralta, J. E.; Ogliaro, F.; Bearpark, M. J.; Heyd, J. J.; Brothers, E. N.; Kudin, K. N.; Staroverov, V. N.; Keith, T. A.; Kobayashi, R.; Normand, J.; Raghavachari, K.; Rendell, A. P.; Burant, J. C.; Iyengar, S. S.; Tomasi, J.; Cossi, M.; Millam, J. M.; Klene, M.; Adamo, C.; Cammi, R.; Ochterski, J. W.; Martin, R. L.; Morokuma, K.; Farkas, O.; Foresman, J. B.; Fox, D. J. Gaussian 16, Revision C.01, Gaussian, Inc., Wallingford CT, **2019**. (c) Cossi, M.; Rega, N.; Scalmani, G.; Barone, V. Energies, Structures, and Electronic Properties of Molecules in Solution with the C-PCM Solvation Model. *J. Comput. Chem.* **2003,** *24,* 669–681. (d) Jusélius, J.; Sundholm, D.; Gauss, J. Calculation of current densities using gauge-including atomic orbitals. *J. Chem. Phys.* **2004**, *121*, 3952–3963. (e) Monaco, G.; Zanasi, R. Assessment of Ring Current Models for Monocycles. *J. Phys. Chem. A* **2014,** *118,* 1673–1683. (f) Steiner, E.; Fowler, P. W. Patterns of Ring Currents in Conjugated Molecules: A Few-Electron Model Based on Orbital Contributions. *J. Phys. Chem. A* **2001**, *105*, 9553–9562. (g) Steiner, E.: Fowler, P. W. Four- and two-electron rules for diatropic and paratropic ring currents in monocyclic π systems. *Chem. Commun.* **2001**, *21*, 2220–2221.